KSCE Journal of Civil Engineering (2023) 27(8):3403-3417
DOI 10.1007/s12205-023-0683-y

pISSN 1226-7988, eISSN 1976-3808
www.springer.com/12205

Structural Engineering

Structural Damage Identification Based on Convolutional Neural Network Group Considering the Sensor Fault

Yongpeng Luo[a], Linkun Wang[b], Xu Guo[a], Jinlin Zheng[a], Feiyu Liao[a], and Zixiong Guo[c]

[a]*School of Transportation and Civil Engineering, Fujian Agriculture and Forestry University, Fuzhou 350002, China*
[b]*Jiangxi Communications Engineering Development Co., Ltd., Nanchang 330038, China*
[c]*Key Laboratory for Structural Engineering and Disaster Prevention of Fujian Province, Huaqiao University, Xiamen 361021, China*

ARTICLE HISTORY

Received 9 May 2022
Revised 1st 28 December 2022
Revised 2nd 11 April 2023
Accepted 11 May 2023
Published Online 24 June 2023

KEYWORDS

Structural health monitoring
Structural damage identification
Sensor fault diagnosis
Convolutional neural networks

ABSTRACT

This article proposes a structural damage identification method based on one-dimensional convolutional neural network group considering sensor faults. The method aims to reduce the damage misjudgment caused by sensor faults. In the proposed method, according to the sensor layout, some convolutional neural network sub-models are established to extract the features from raw vibration data for sensor fault diagnosis and structural damage identification; then two convolutional neural networks groups, namely the sensor fault diagnosis group and the damage identification group are designed on the basis of the functions of each sub-model. The sensor fault diagnosis group determines whether the sensor data is abnormal and truncates the abnormal signal. The remaining normal signal are entered into the damage identification group and the final damage identification results are calculated according to the statistical decision module. The effectiveness of the devised method is verified by the IASC–ASCE benchmark structure and laboratory experiments. The results demonstrate that the sensor fault diagnosis and damage identification accuracy of each sub-model ranges from 98.54% to 99.77% and from 87.21% to 91.74% respectively at different noise levels; the damage identification group can reduce the impact of sub-model misjudgment on the structural damage identification. The accuracy of the final damage identification results is 100%. The identification time of all samples in the test set is 53.09 s and 22.93 s, respectively, for SHM benchmark and Laboratory experiment cases. And the average judgment time of each submodel in the sensor fault diagnosis group was 278 and 94 ms, and that of each submodel in the damage identification group was 294 and 105 ms, respectively, for a single test sample, which fulfills the requirements of online damage identification for structural health monitoring.

1. Introduction

The performance of engineering structures inevitably deteriorates in long-term service periods under environmental erosion, material aging, working load, and other factors. As a result, their ability to resist natural disasters and even typical environmental effects is reduced, which leads to catastrophic emergencies in extreme cases (Altunışık et al., 2019; Chi et al., 2021; Ananthi et al., 2022). Consequently, ensuring the health of engineering structures in real-time has become a crucial research topic (Zhu et al., 2011; Flouri et al., 2012; Ding et al., 2018). The health monitoring of structures chiefly detects structural damage or degradation by analyzing structural system characteristics, including the structural response (Hüsem et al., 2018; Ananthi et al., 2021). The accuracy of the evaluation results strongly depends on the sensors and the interpretation algorithm (Kahya et al., 2021). It is worth noting that sensors have an average lifespan of approximately 10 years, but the lifespan of bridge structures can be more than 100 years. Therefore, during the service period of bridges, sensors may degrade or even fail (Li et al., 2008). Unfortunately, sensor fault, noise, and external disturbances can also cause abnormal variations masking signals from the actual structural damage (Kullaa, 2010;

CORRESPONDENCE Yongpeng Luo ✉ yongpengluo@fafu.deu.cn 🏢 School of Transportation and Civil Engineering, Fujian Agriculture and Forestry University, Fuzhou 350002, China

Li et al., 2020).

According to different data processing methods, Frank (1996) divided the algorithms for sensor fault diagnosis into three categories: the algorithms based on analytical models, signal processing, and knowledge. The approach based on analytical models is suitable for sensor systems that can establish an accurate linear model, which can realize rapid diagnosis with a sound effect. However, it is challenging to establish an accurate model for complex civil engineering structures (Mohamed and Ibrahim, 2002), which limits the application and development of such methods in structure health monitoring system. The method based on signal processing can directly analyze signals without distinguishing fault types and causes of the faults, but its detection results depends on the signal analysis method (Li et al., 2019).

Alternatively, as a novel type of machine learning, deep learning has attracted extensive attention from academic, which aims to extract abstract and valuable information from data via stacking multiple non-linear processing layers in hierarchical architectures, and therefore, is more powerful than those traditional intelligent methods (Zhao et al., 2019). Fu et al. (2019) presented a three-stage strategy to autonomously detect, identify, and recover sensor faults, the benefits and limitations of this strategy are discussed. Liu et al. (2020) proposes a deep learning-based method, namely, the Tsfresh Long Short-Term Memory networks, to address the sensor fault classification. Jana et al. (2022) introduced Convolutional Neural Network (CNN) and Convolutional Autoencoder to identifies the presence and type of fault in sensor data, location of the faulty sensor.

In the field of structural damage identification, deep learning has also received extensive attention (Azimi et al., 2020; Zhang et al., 2020). Li et al. (2020) proposed a fully connected stateful long short time memory (FS-LSTM) Neural Networks for differentiating the sensor fault and structural damage without information on details of the fault. Compared with LSTM, a convolutional neural network can independently learn the real-time monitoring data on a structure at a low computing cost. Zhan et al. (2021) discussed the performance of structural damage detection based on CNN under the influence of the randomness of structural parameters. Lin et al. (2017) also presented a method that used the wavelet packet component energy as the feature vector to be substituted into the one-dimensional CNN model to identify structural damage. Their experimental results showed that the proposed method had good performance due to its noise resistance and ability to locate damage.

As mentioned earlier, deep learning has gradually been applied to sensor fault diagnosis and damage identification and has achieved good results. However, there is still no good solution to effectively distinguishing the response changes caused by the sensor faults from those caused by structural damage. Therefore, this study devised a novel method of structural damage identification based on a one-dimensional convolutional neural network group considering sensor fault. First, some sub-models for shallow sensor fault diagnosis and deep structural damage identification were established to automatically extract features from sensor data. According to the functions of each sub-model, the sensor fault diagnosis group (SD-CNN group) and the damage identification group (DI-CNN group) were designed to perform layer-by-layer sensor fault diagnosis and damage identification using data sets. Finally, the specific performance and robustness of the developed method were analyzed and discussed through the numerical simulation of the IASC–ASCE benchmark structure and the laboratory experiment.

2. Theory of Structural Damage Identification Considering Sensor Fault

2.1 Sensor Faults

According to the existing works (Kullaa, 2011; Kullaa, 2013), the deviation of the signal in faulty instruments may be described mathematically in terms of bias, drifting, precision degradation, gain, and constant. The mathematical expression is shown in Table 1. In Table 1, $u[t]$ is the time series including the fault of the sensor calculated by the sensor fault model; t represents the number of sampling points; $\hat{u}[t]$ indicates the dynamic response of the healthy sensor; $w[t]$ stands for the Gaussian white noise sequence used to simulate the environmental noise interference.

In the actual use of the sensor, due to the change of the position of the sensor, its own output value and the real value appear quantitative deviation, resulting in the bias phenomenon. At the same time, when the sensor is completely faulty, the output value is often fixed or composed of white noise. Therefore, the unknown constant A is set to simulate the constant value when the sensor is bias and completely faulty. However, in drifting and precision degradation, drift and precision degradation may be random variables, so a random number η in the range of [0,1] are set together with unknown constants B and C to define drifting and presision degradation. In addition, the sensor gain fault may occur due to the unstable voltage supply of the sensor. The unknown constant G in Table 1 is the gain coefficient. When the gain coefficient G increases, the sensor accuracy decreases as well.

2.2 Architecture of Convolution Neural Network

This section interprets the architecture of the designed convolution neural network and introduces the function and background of each layer. The fundamental structure of the CNN chiefly comprises an input layer, convolutional layers, pooling layers, and an output layer (Long et al., 2015). The following is a brief introduction to

Table 1. Sensor Faults Model

Fault type	Mathematical expressions
Bias	$u[t] = A + \hat{u}[t] + w[t]$
Drifting	$u[t] = A + B \times t + \hat{u}[t] + w[t]$
Precision degradation	$u[t] = C \times \eta + \hat{u}[t] + w[t]$
Gain	$u[t] = G(\hat{u}[t] + w[t])$
Constant	$0/A/w(t)$

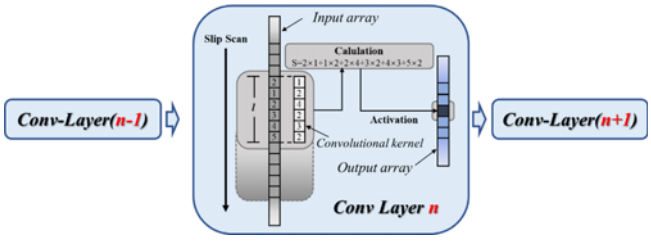

Fig. 1. The Sliding Scan and Convolution Calculation

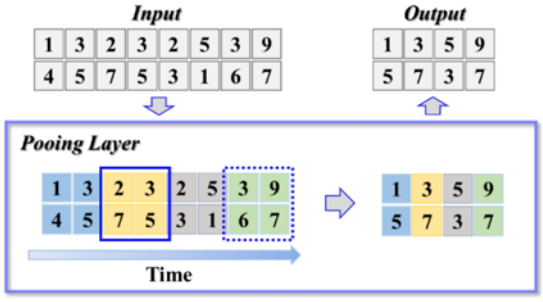

Fig. 2. The Process of the Max Pooling

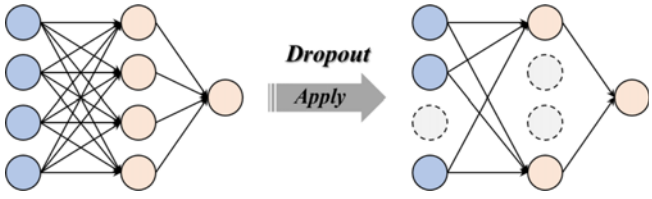

Fig. 3. The Process of the Dropout Layer

the theory of convolution neural network.

2.2.1 Convolutional Layer

As the core layer of the one-dimensional CNN, the convolutional layer is primarily used for feature extraction in the input array through sliding scanning and inner product operation, as shown in Fig. 1. In this network layer, n convolutional kernels are given an initialization and a corresponding random array based on an artificially specified time-domain window size of l. The input array in the time-domain window is subsequently multiplied and summed with the elements of the convolution kernel to obtain the output value.

As simple multiplication and summation are linear calculations, they do not effectively improve the representation of the network model. Therefore, a nonlinear mapping using an activation function during the contact between the convolution kernel and the data is used, which alleviates the problem of gradient disappearance caused by slow parameter updating during the model training. Hence, given the higher performance of the rectified linear unit (ReLU) function, this study chooses it as the activation function for this model in the classification problem (Krizhevsky et al., 2012); the ReLU activation function is expressed by:

$$f_{\mathrm{ReLU}}(x)=\begin{cases}0, x\le 0\\ x, x>0\end{cases}, \tag{1}$$

where x is the input data after the inner product, and the output data, $f_{\mathrm{ReLU}}(x)$: are recombined in the order of the data before the calculations.

Furthermore, the n convolution kernels often transform the array at a specific sliding interval (k) throughout the traversal process and then transform the matrix with the dimensions $m \times 1$ into an output matrix with the dimensions $[(m-l)/k+1] \times n$ in the next convolutional layer for convolutional computation or in other types of network layers for data processing.

2.2.2 Max Pooling Layer

As the convolution calculation proceeds, the input array is transformed gradually into a large-scale data feature matrix. To improve the computational efficiency of the model, we set up a one-dimensional max-pooling layer between adjacent convolutional layers to perform data selection in the input array. As depicted in Fig. 2, the input matrix entering the pooling layer is divided into several matrices along the time axis, and the maximum value of the elements in the resulting matrix is used as the elements in the output matrix. The pooling layer reduces the amount of data by decreasing the dimension of the data and thus controls the occurrence of overfitting. Despite the reduction in the amount of data, the feature information of the matrix is not lost due to the computational impact of the pooling layer, ensuring that the final generated model is still relevant.

2.2.3 Dropout Layer

On the basis of the complexity of the network layers in the convolutional neural network model, Srivastava et al. (2014) proposed the dropout technique to better prevent overfitting of the model. As depicted in Fig. 3, the dropout method randomly and temporarily zeroes some elements of the feature map during the training, indicating that some matrix elements are invalidated. It ensures that the network model is not overly dependent on particular local features during the training and enhances the generalization ability of the model. At the same time, the failed elements are reactivated in the subsequent intersection validation phase, improving the convergence performance of the model. In general, dropout reduces overfitting during the training phase by reducing the complexity of the model.

2.2.4 Output Layer

With the calculation of the convolution, pooling, and dropout layers, the CNN model determines the output matrix with local features, that is, $\boldsymbol{A}_{a\times b\times c}$. In order to facilitate the output of the classification results of the subsequent model, we set up two network layers, namely a fully connected (FC) layer and a softmax layer, in the output layer of the CNN for processing and analysis. First, the input matrix ($\boldsymbol{A}$) is tiled and expanded in the FC layer and transformed into a one-dimensional array of size $(a \times b \times c) \times 1$. The element u in the array is reorganized twice by Eq. (2) to obtain one-dimensional array $\boldsymbol{V}$ with the

dimensions $m \times 1$.

$$\boldsymbol{V} = f_{\mathrm{ReLu}}\left(\sum u \times w + b\right), \tag{2}$$

where m is the manually specified output dimension, w denotes the $(a \times b \times c) \times m$ weight parameters corresponding to the node, and b represents the m bias parameters.

Finally, array $\boldsymbol{V}$ enters the softmax layer and reverts to the one-dimensional array $\boldsymbol{S} = [\mathrm{S}_1\ \mathrm{S}_2\ \ldots\ \mathrm{S}_m]$ through Eq. (3):

$$\mathrm{S}_i = \frac{e^{V_i}}{\sum_j e^{V_j}}, \tag{3}$$

where e^{V_i} is the index of an element, and $\sum_j e^{V_j}$ indicates the sum of the indices of all the elements. The softmax layer pools the output value of S_i in Eq. (3) for each element value in array $\boldsymbol{V}$ (V_i). Each element of $\boldsymbol{S}$ (S_i) represents the probability of each condition, so the condition with the maximum probability is obtained. After evaluating and comparing predicted probabilities, the element with the highest probability is used as the final model classification result and output in the test phase. When the model is in the training stage, the model uses cross entropy (Boudiaf et al., 2020) as the loss function to calculate the deviation between the CNN output result and the label result, which is used for model cycle iteration. At the same time, in this paper, combining adaptive moment estimation (adam) (Kingma and Ba, 2015) is used to participate in the continuous optimization and training of the model to minimize the loss function and obtain the optimal model.

2.3 Sensor Fault Diagnosis and Structural Damage Identification

The proposed method identifies the sensor state and structural damage by the SD-CNN group and the DI-CNN group, as shown in Fig. 4. Before the model training, the original data collected by the sensor will be cut according to the preset input size of the submodel to complete the data set establishment. Andthen the SD-CNN group determines the anomalous signal and truncates it into the DI-CNN group before identifying the damage, enhancing the accuracy of structural damage identification in sensor-based networks. The method employs multiple parallel one-dimensional CNN submodels to achieve a global view of the sensor network, effectively clarifying the characteristics of the raw data collected by each sensor and training a reliable model for subsequent diagnosis and identification.

2.3.1 Architecture of Submodels of SD-CNN Group and DI-CNN Group

The SD-CNN group and the DI-CNN group consist of n one-dimensional CNN submodels corresponding to n acceleration sensors. The CNN models can have different classification performances depending on the combination of the network layers and the activation functions. In general, as the depth of the convolutional layer model increases, the feature extraction capability of the CNN improves, but too many convolutional layers can lead to overfitting and reduce the actual performance of the model. Therefore, each submodel of the SD-CNN group is equipped with six convolutional layers and three pooling layers after the preliminary trial calculations. A varying number of one-dimensional convolutional kernels with time-domain window sizes of 16, 4, and 2 are utilized to extract features from the input signal in turn. The feature matrix is then recursively moved to the deeper layers while the 2-D feature matrix is converted to a one-dimensional matrix before entering the output layer; finally, the calculation of the softmax function determines the prediction result of the input signal. Fig. 5 illustrates the network structure.

Convolutional kernels with similar time-domain window sizes are set for processing the data in the DI-CNN group since the signal, at its input, has the same size as the SD-CNN group submodels. Furthermore, considering the distribution of the different features of the feature matrix data used for sensor fault diagnosis and structural damage identification, we construct the DI-CNN group submodel with eight layers of convolutional kernels and four layers of pooling layers, as illustrated in Fig. 6.

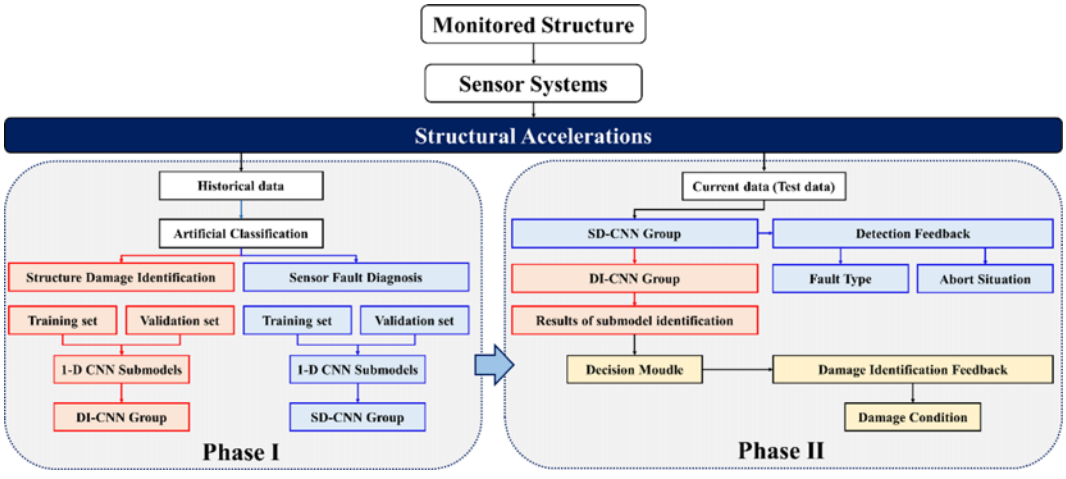

Fig. 4. The Flow Chart for the Proposed Method

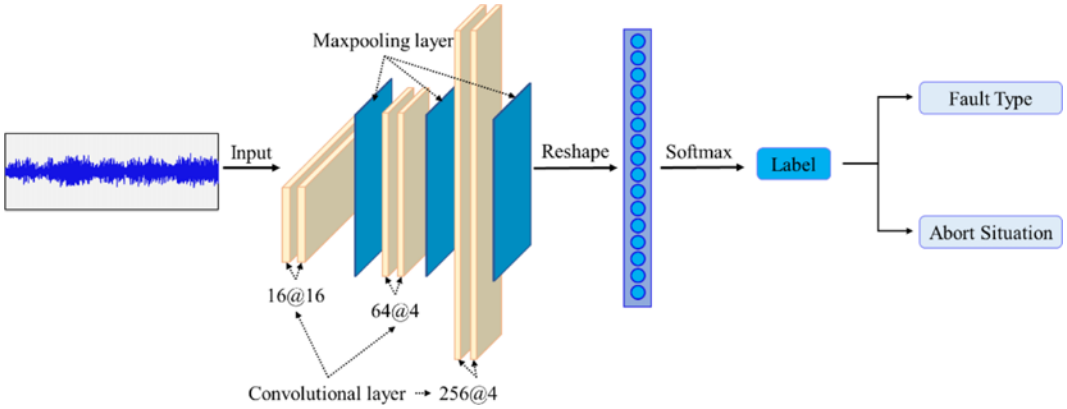

Fig. 5. The Architecture of the Submodel of the SD-CNN Group

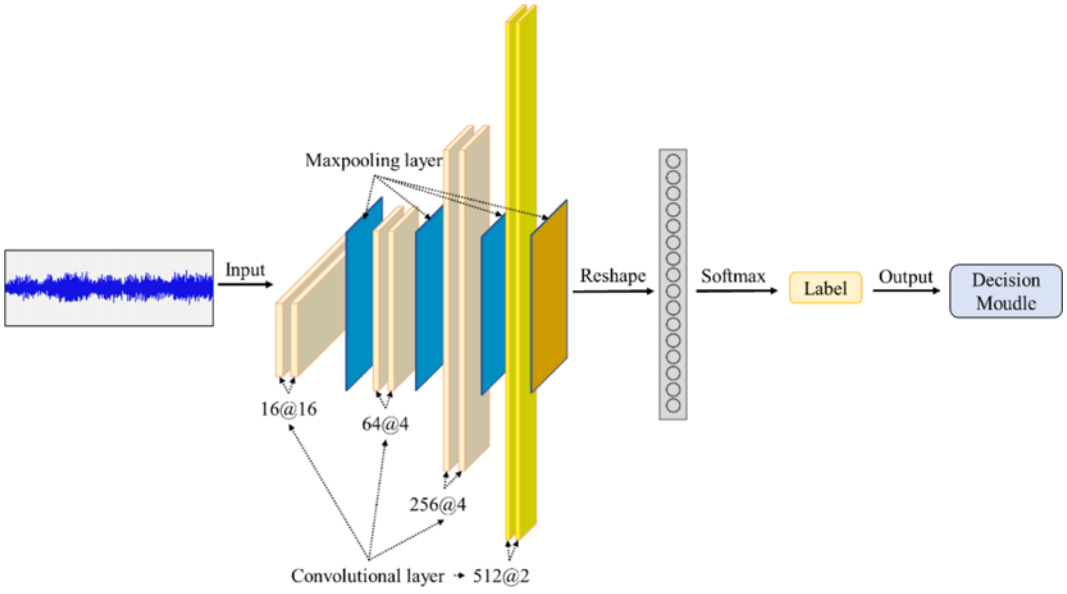

Fig. 6. The Architecture of the Submodel of the DI-CNN Group

2.3.2 Process of Structural Damage Identification Considering Sensor Fault

First, the SD-CNN group and the DI-CNN group are constructed according to the above submodels. After the input data are passed through the shallow SD-CNN group, array $\boldsymbol{C} = [C_1\ C_2\ \ldots\ C_k\ \ldots\ C_n]$ containing information about both the channel and the performance state of the sensor is output. If the information stored in element C_k indicates that the faulty sensor is abnormal, the signal is truncated into the deep DI-CNN group, enabling the faulty sensor to be found and the fault class to be detected. On the basis of the output information of the shallow group ($\boldsymbol{C}$): the DI-CNN group continues to recognize the input data and generates the array $\boldsymbol{D} = [D_1\ D_2\ \ldots\ D_k\ \ldots\ D_n]$, where D_k is the output of each one-dimensional CNN submodel for structural damage identification after the diagnosis and recognition of the two layers of one-dimensional CNN group. To eliminate the effects of the misjudgments of individual submodels as much as possible, we set up the decision module to generate array $\boldsymbol{K}$ composed of the predictions of each category by counting the results and determining the maximum value of K_i as the final assessment result of the target structural damage category. The details are as follows:

$$K_i = \max\{K_1, K_2, \ldots, K_k, \ldots, K_l\}, \tag{4}$$

where K_k indicates the specific number of submodels, the discriminant result of which is condition k; l denotes the number of conditions available in the sample library of the structural damage.

3. Experimental Phase I of SHM Benchmark Data

The records of experimental phase I of the IASC–ASCE structural health monitoring (SHM) benchmark problem (Johnson et al., 2004) are utilized in the present study. The benchmark frame is a four-story steel structure built at the University of British Columbia. The footprint dimensions are 2.5 m × 2.5 m, and the height of the frame is 3.6 m. Two parallel steel rods are installed diagonally at each bay to provide bracing.

Table 2. The Description of the Damage Patterns in the IASC–ASCE Benchmark Problem

Labels	Damage pattern
1	Undamaged
2	Remove all braces in the first story
3	Remove all braces in the first and third stories
4	Remove one brace in the first story
5	Remove one brace in each of the first story and the third story
6	Remove one brace in each of the first story and the third story and loosen the floor beam at the first level
7	2/3 stiffness in one brace in the first story

As presented in Table 2 and Fig. 7, six structural damage patterns were simulated on the benchmark frame. For each case, the acceleration output was recorded by 16 accelerometers under ambient excitation, and the acceleration measurements for all damage patterns were sampled at 500 Hz; the recording time was 10 s. Fig. 8 shows the location of the accelerometers. The noise was also added to the original signals at different signal-to-noise ratios to simulate the interference of environmental noise and other factors. Five types of data sets with noise levels of 10%, 20%, 30%, 40%, and 50% were generated by noise addition and expansion for the training. Further, a data set of size 1400 × 5000 was generated for each of the 16 measurement points, where 5000 was the length of the 10-second signal fragment generated by adding noise simulation and 1400 was the total number of signal fragments under the 7 damage patterns. The obtained data sets were further divided to obtain the train set, validation set and test set for the subsequent experiment, among which the proportions of three types of data sets were 60%, 20% and 20% respectively.

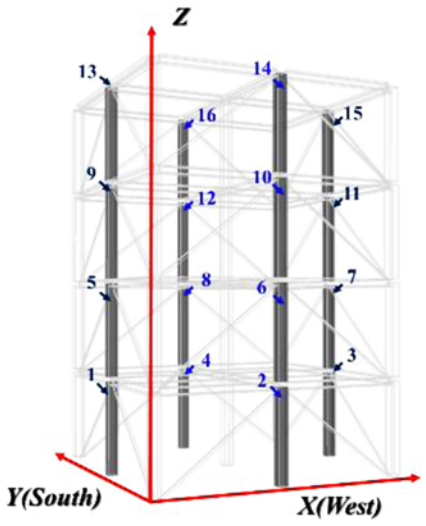

Fig. 8. The Locations of the Sensors

3.1 Studying Sensor Fault Diagnosis Based on Submodel in SD-CNN Group

The five different types of sensor faults discussed in Section 2.1 were studied, and the benchmark structure was assumed to be in a healthy state. A total of six scenarios were studied, including five scenarios with a single fault in the sensor and one scenario without any fault, as presented in Table 3. To study the influence of the degree of sensor fault on diagnosis results, two fault levels was employed to describe the degree of sensor fault based on the mean, standard deviation of the input sample (δ). Magnitude S represents the lower level of the sensor fault, and N indicates the duration of the fault signal.

Figure 9 delineates the training process of sensors 1# and 2# at a magnitude of S. The trend of the loss value obtained during

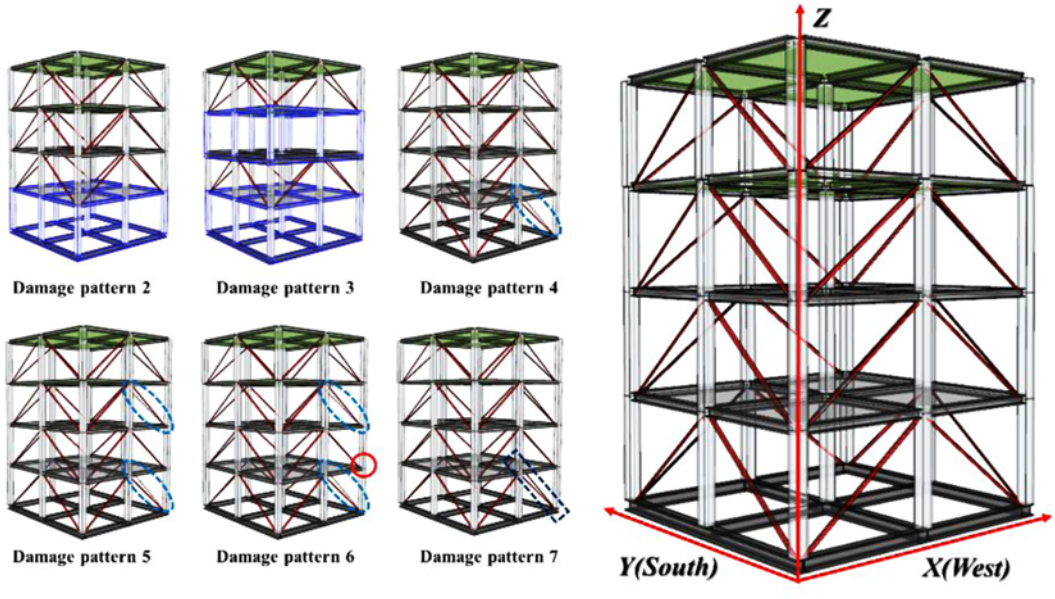

Fig. 7. Damage Patterns 2 to 7

Table 3. The Mathematical Expressions of Five Types of Sensor Faults

Fault type	Label	Mathematical expressions	Parameter ($\delta = 1.4330$)	k	
				S	M
Healthy	1	/	/	/	/
Bias	2	$u[t] = A + \hat{u}[t] + w[t]$	$A = k\delta$	0.25	0.50
Constant	3	$0/A/w(t)$	$A = k\delta$	0.01	0.1
Drifting	4	$u[t] = A + B \times t + \hat{u}[t] + w[t]$	$A + BN = k\delta$	0.25	0.50
Precision degradation	5	$u[t] = C \times \eta + \hat{u}[t] + w[t]$	$C = k\delta$	0.25	0.50
Gain	6	$u[t] = G(\hat{u}[t] + w[t])$	$G = k$	1.20	0.70

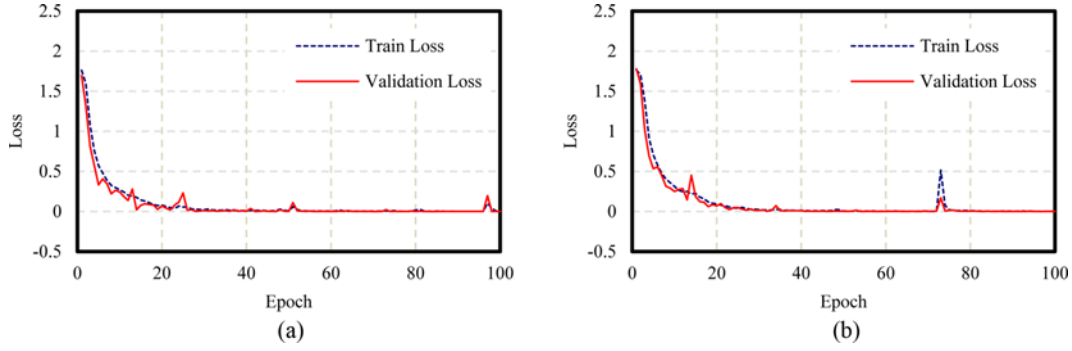

Fig. 9. The Variation in the Loss Value of the SD-CNN Submodels: (a) Sensor 1#, (b) Sensor 2#

the convergence of the model determines whether the model continues to learn or has finished converging. As seen in the figure, the SD-CNN submodels of both sensors show a sharp decline in the loss value at the beginning of the training; as the number of iteration cycles gradually increases, the loss value gradually approaches zero, implying that the model has converged and can be used for the subsequent test.

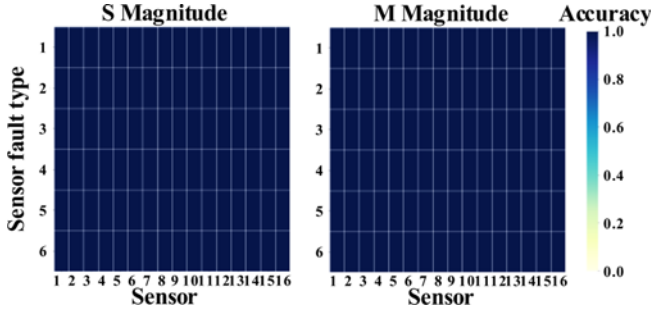

Fig. 10. The Accuracy of the SD-CNN Submodels at Magnitudes of *S* and *M* at a 10% Noise Level

Figure 10 depicts the accuracy of the SD-CNN submodels at magnitudes of *S* and *M* at a noise level of 10%. The SD-CNN models have solid diagnosis performance in the range of the proposed magnitudes. The 16 SD-CNN submodels achieve an average degree of accuracy of 100% for identifying 6 categories of the sensor fault models using the testing datasets with magnitudes of *S* and *M*. Fig. 11 depicts the results of the fault diagnosis for each sensor at different noise levels and a magnitude of *S*. The recognition ability of the SD-CNN submodels decreases as the degree of noise interference rises. The diagnostic model for sensor 5# identified the gain data with an accuracy of 45.28% at a noise level of 40%, and the diagnostic model for sensor 13# identified the health data with an accuracy of 40% at a noise level of 50%; however, they are still robust to a certain extent.

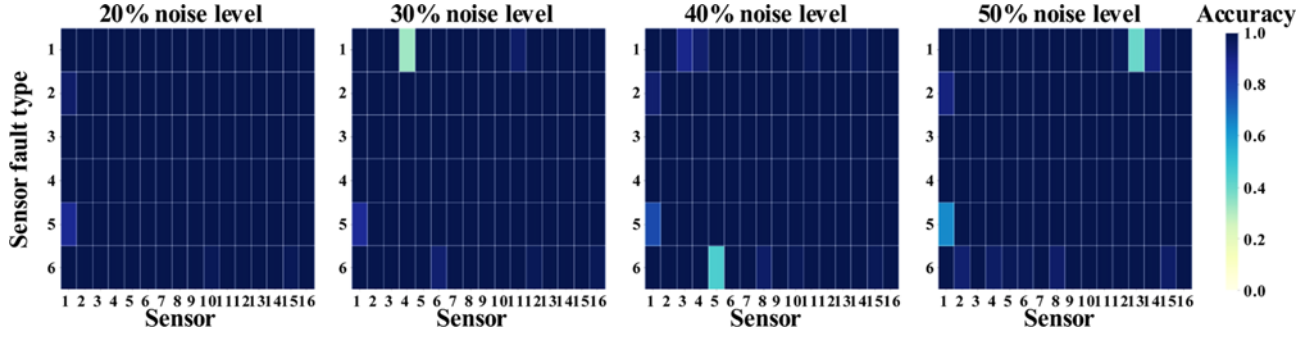

Fig. 11. The Detection Accuracy of the SD-CNN Submodels at Various Noise Levels

Table 4. The Detection Accuracy of the RF Algorithm at Various Noise Levels

Sensor location	10% noise level	20% noise level	30% noise level	40% noise level	50% noise level
Sensor1	1.00	0.96	0.94	0.91	0.91
Sensor2	1.00	0.99	0.96	0.97	0.94
Sensor3	1.00	0.99	0.99	0.97	0.98
Sensor4	1.00	0.98	0.96	0.97	0.96
Sensor5	0.99	0.99	0.95	0.95	0.95
Sensor6	1.00	0.99	0.98	0.96	0.96
Sensor7	1.00	0.98	0.98	0.97	0.96
Sensor8	0.99	0.99	0.98	0.97	0.95
Sensor9	1.00	1.00	0.96	0.96	0.95
Sensor10	0.99	0.99	0.97	0.96	0.96
Sensor11	1.00	0.99	0.97	0.97	0.96
Sensor12	0.99	0.99	0.97	0.95	0.94
Sensor13	0.98	0.96	0.95	0.94	0.90
Sensor14	1.00	0.99	0.98	0.95	0.91
Sensor15	0.99	0.98	0.97	0.93	0.94
Sensor16	1.00	0.97	0.94	0.93	0.91

The average degree of the accuracy of the SD-CNN submodels remains in the range of 98.54% – 99.77%.

The random forest (RF) algorithm is used to fault diagnosis for each sensor at different noise levels and a magnitude of S, and the diagnosis results are shown in Table 4. Fig. 12 shows a comparison between the results of the RF and the proposed algorithm. It can be seen from Table 4 and Fig. 12, the diagnosis accuracy of the proposed algorithm is higher than that of the RF algorithm at five noise levels. With the increase of noise level, the average accuracy of sensors in the proposed algorithm is greater than 0.99, while the average accuracy of RF algorithm is 0.94. In conclusion, the diagnosis accuracy of the proposed algorithm is better than that of the RF algorithm.

3.2 Studying Damage Identification Based on Submodel in DI-CNN Group

The seven different types of damage patterns listed in Table 2

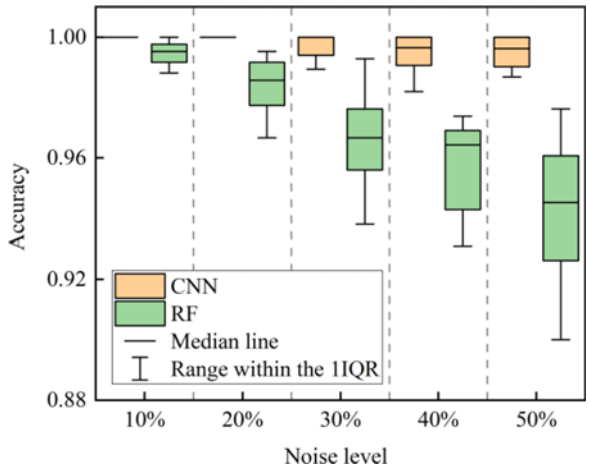

Fig. 12. Comparison of Diagnosis Accuracy between CNN and RF at Various Noise Levels

were studied, and the sensor was assumed to be in a healthy state. The construction of the DI-CNN group also consisted of 16 submodels corresponding to the number of measurement points of the target structure. According to the supervised learning characteristics of the CNN, each submodel of the DI-CNN group was determined based on the data samples of size 1120 × 5000 obtained from the measurement points and was continuously cross-trained by the training and validating sets. Fig. 13 displays the damage identification ability of each one-dimensional CNN submodel in the testing set at various noise levels. Each one-dimensional CNN submodel in the DI-CNN group presents good recognition results for the data samples at all noise levels, and the average recognition accuracy of the submodels is 91.74%, 91.68%, 89.88%, 88.54%, and 87.21% at a noise level of 10%, 20%, 30%, 40%, and 50% respectively, which confirms the excellent resistance of the DI-CNN group submodels to noise.

The RF algorithm is also used to re-identify the structural damage, and the identification results are shown in Table 5. Fig. 14 shows a comparison between the results of the RF and the proposed algorithm. It can be seen from Table 5 and Fig. 14, the identification accuracy of the proposed algorithm is higher than that of the RF algorithm at five noise levels. With the increase of noise level,

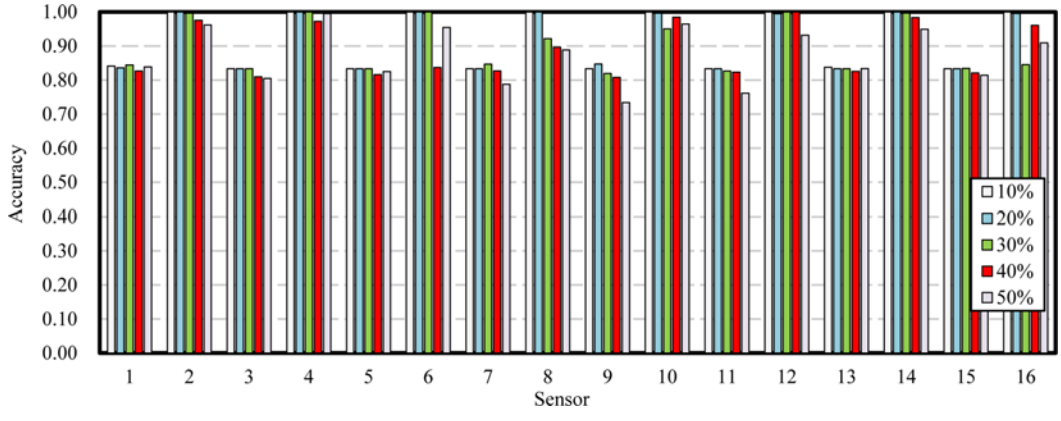

Fig. 13. The Structural Damage Identification Accuracy of Each Submodel at Various Noise Levels

Table 5. The Structural Damage Identification Accuracy of the RF Algorithm at Various Noise Levels

Sensor location	10% noise level	20% noise level	30% noise level	40% noise level	50% noise level
Sensor1	0.80	0.77	0.67	0.64	0.60
Sensor2	0.86	0.89	0.85	0.83	0.70
Sensor3	0.84	0.84	0.86	0.81	0.74
Sensor4	0.93	0.86	0.85	0.83	0.85
Sensor5	0.85	0.85	0.78	0.75	0.72
Sensor6	0.94	0.91	0.84	0.87	0.85
Sensor7	0.74	0.66	0.61	0.59	0.56
Sensor8	0.90	0.85	0.75	0.68	0.58
Sensor9	0.80	0.66	0.60	0.55	0.62
Sensor10	0.97	0.90	0.84	0.79	0.74
Sensor11	0.78	0.75	0.70	0.64	0.56
Sensor12	0.96	0.89	0.84	0.83	0.77
Sensor13	0.85	0.80	0.72	0.68	0.58
Sensor14	0.96	0.91	0.84	0.79	0.74
Sensor15	0.74	0.73	0.63	0.61	0.61
Sensor16	0.94	0.91	0.89	0.75	0.79

the average accuracy of sensors in the proposed algorithm is greater than 0.87, while the average accuracy of RF algorithm is 0.69. In conclusion, the identification accuracy of the proposed algorithm is better than that of the RF algorithm.

3.3 Multisensor Fault Diagnosis and Damage Identification Results

Three mixed scenarios with simultaneous damage and sensor failure were set, as shown in Fig. 15. In mixed scenario-1, the structural damage was described as "remove all braces in the first story"; Sensors 1#, 6#, 8#, 11#, and 16# were set as bias, constancy, drift, loss of accuracy, and gain respectively. The noise level was set at 20%, and the degree of the sensor fault was *S*-level. Fig. 16 presents the time curves under mixed scenarios.

Figure 17 shows the sensor fault diagnosis results of the three mixed scenarios, where red indicates that the sensor fault diagnosis result is wrong. Compared to the actual fault types depicted in Fig. 15, the accuracy of the sensor fault judgment results is high, and only some sensor fault classification is wrong. On the basis of the detection results of the sensor fault in the three simulation

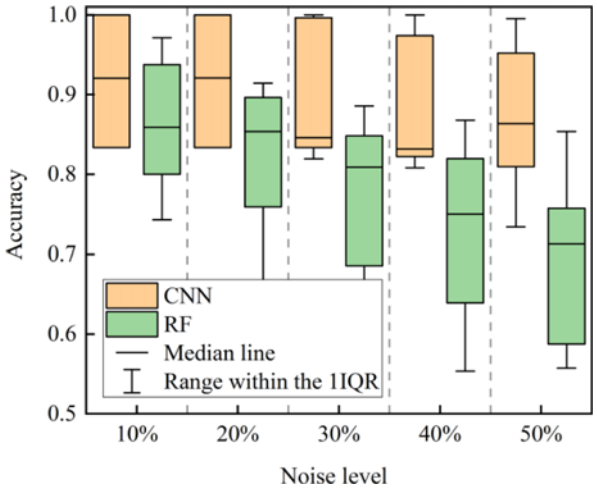

Fig. 14. Comparison of Structural Damage Identification Accuracy between CNN and RF at Various Noise Levels

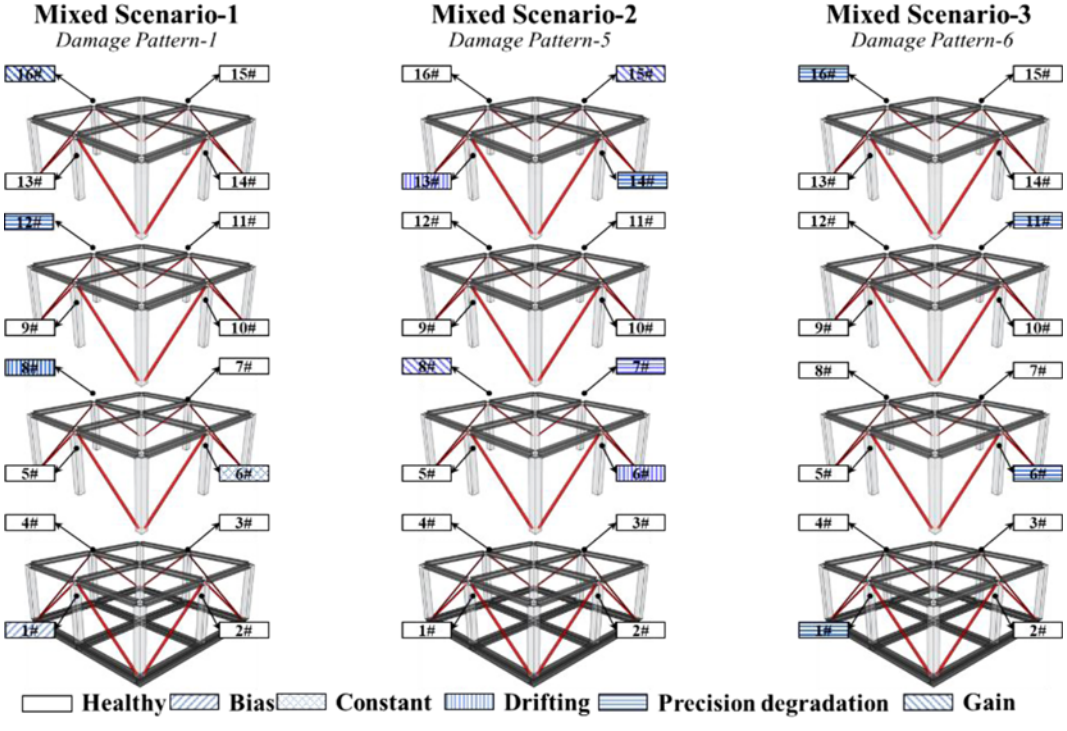

Fig. 15. A Schematic of the Settings of the Mixed Scenarios

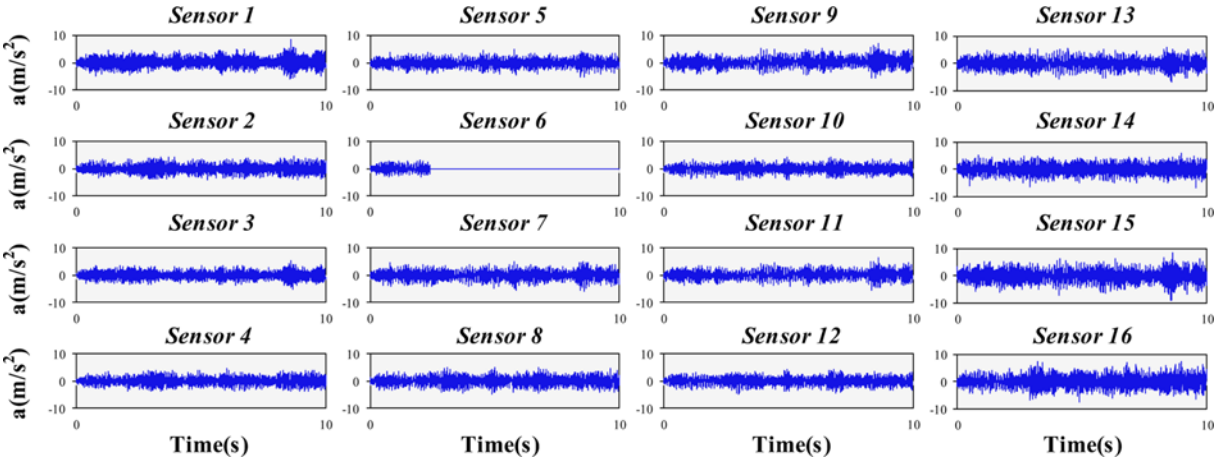

Fig. 16. The Acceleration Time History Curve (mixed scenario-1)

scenarios in Section 3.2, the proposed algorithm can reduce graphics processing unit (GPU) usage by switching off the input channels of the faulty signals. The number of the input channels of the DI-CNN group is reduced from 16 to 11, 10, and 12. The remaining fault-free sensor signals are fed into the DI-CNN group and combined with the final damage identification results by the decision module, as shown in Fig. 17, in which the decision module and the final results obtained from the SD-CNN group and the DI-CNN group are on the left, and the DI-CNN submodel alone is on the right. The comparative analysis of the recognition results reveals that the sensor fault can lead to the misclassification of the structural damage, as displayed in Fig. 17(b) for sensors 7# and 8# after incorporating the sensor fault model. In addition, the recognition accuracy of each submodel varies with different noises, which may give rise to misclassification during the detection process, as shown in Fig. 17(a) for sensors 9# and 13#. The decision module statistically calculates the final results of the DI-CNN group to provide an accurate assessment of the state of the structure, reducing the impact of misclassification caused by a single model.

For the testing data sets, the average computation time based on the GTX 950 graphics card is 53.09 s due to the low requirement of computational resources and better adaptability of the one-dimensional CNN submodel. The average computation times of the SD-CNN group and the DI-CNN group are 23.50 and 30.59 s respectively, and the average computation times of the two types of submodels are 278 and 294 ms.

4. Laboratory Experiments on Simply Supported Girder Bridge

A single-span simply supported girder bridge was conducted in the laboratory, as illustrated in Fig. 18. This test structure is composed of two longitudinal beams with a 3.6-m length, four crossbeams with a 1.2-m length and four columns with a 1.0-m length. The cross-section of beam and columns are the Universal Beams (UB) 100 × 100 × 8 × 8 section. Each crossbeam is connected to the longitudinal beams by two plates, using a total of 32 10-mm bolts for each typical connection. And each crossbeam is made of 2 UB beams joined together by two plates and 12 10-mm bolts. Each longitudinal beam is made of 6 UB beams joined together by two plates and 12 10-mm bolts. The supports of the structure were designed as semi-rigid support using neoprene pads.

The modal test was carried out using environmental excitation and Eight piezoelectric accelerometers. The location of the

Table 6. The Design of the Mixed Scenarios

Mixed scenario	Damage pattern	Sensor fault model
1	Healthy	Sensor 1# (drifting) and sensor 2# (precision degradation)
2	Relaxing the connecting plate between nodes 6 and 7	Sensor 1# (drifting) and sensor 3# (drifting)
3	Component damage between nodes 6 and 7	Sensor 1# (precision degradation) and sensor 7# (precision degradation)

Table 7. The Design of the Sensor Fault Model

Sensor fault type	Damage pattern	Mathematical expressions	Parameter
Healthy	1/Healthy	-	-
Drifting	2	$u[n] = A + B \times \eta + \hat{u}[n] + w[n]$	$A = 0, B = 0.002$
Precision degradation	3	$u[n] = C \times \eta + \hat{u}[n] + w[n]$	$C = 0.05$

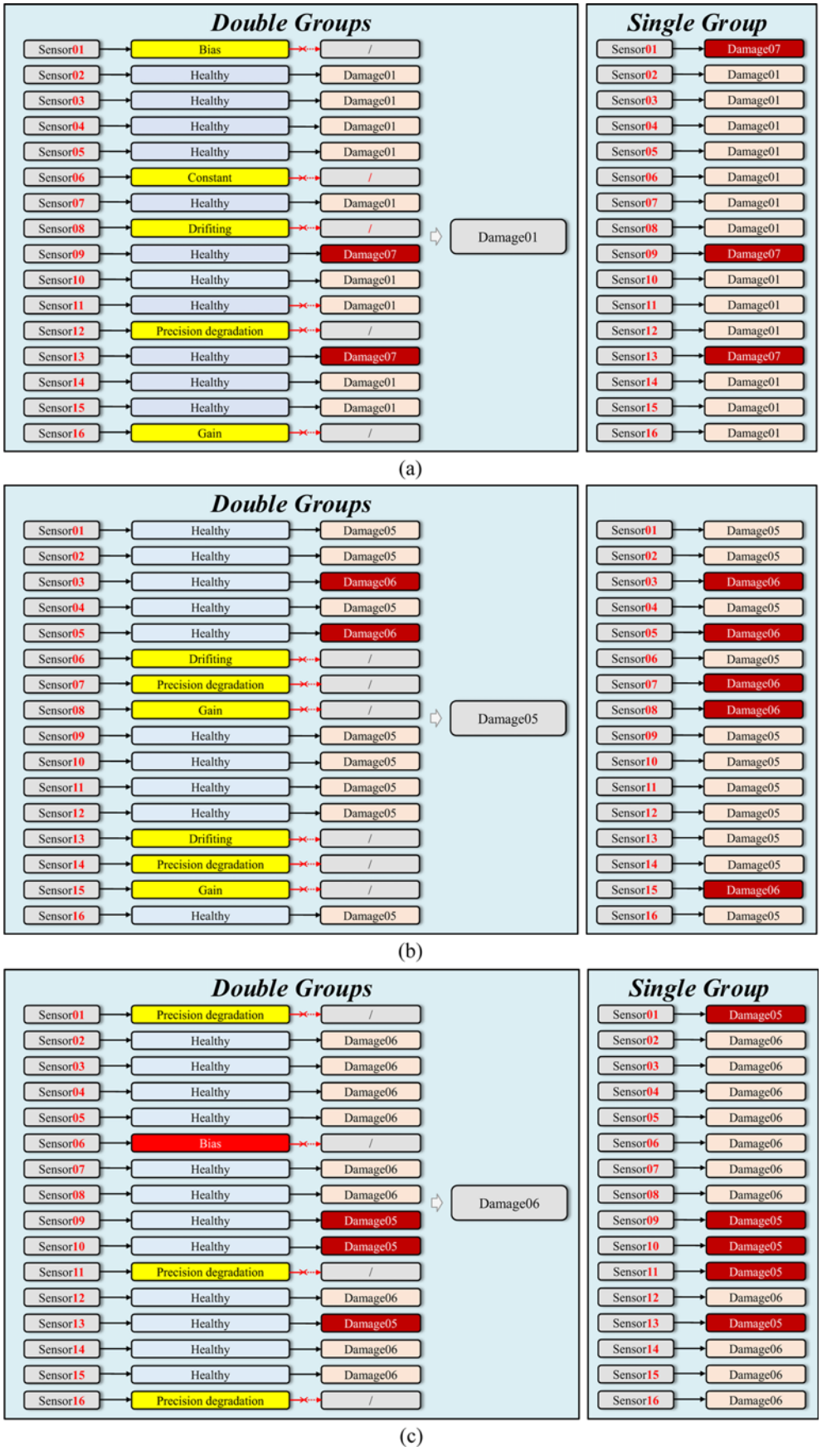

Fig. 17. The Results of the Structural Damage Identification: (a) Mixed Scenario-1, (b) Mixed Scenario-2, (c) Mixed Scenario-3

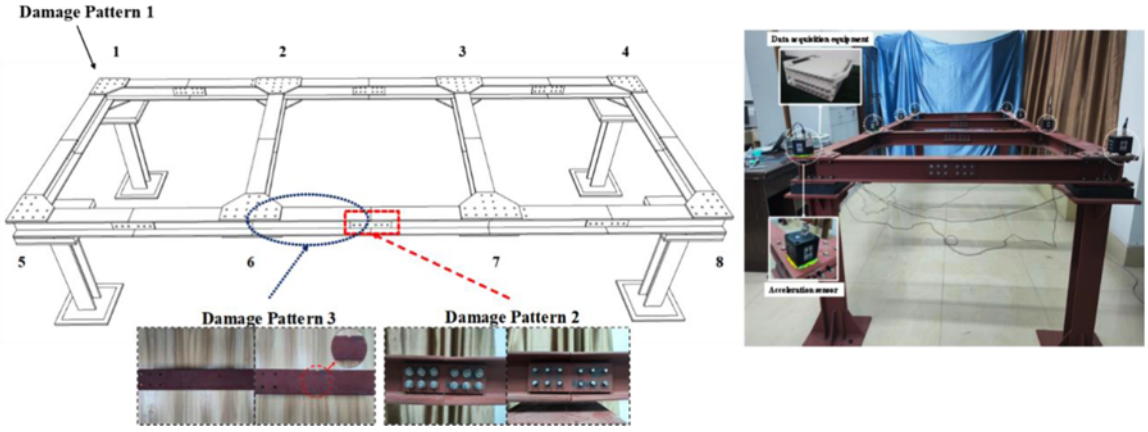

Fig. 18. The Description of the Experimental Platform

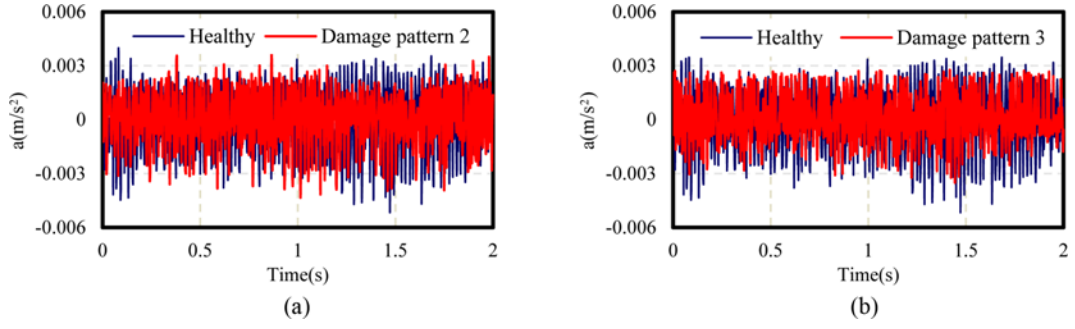

Fig. 19. The Acceleration Time Course Curves: (a) Damage Patterns 2, (b) Damage Patterns 3

accelerometers can be shown at Fig. 18. Eight data samples from Eight accelerometers can be obtained per damage pattern . Based on our preliminary study on this structure, the sampling rate is set as 500 Hz, which is more than enough to cover the first three natural frequencies of the test structure. The Sampling duration is set as 600 s.

In this work, Three mixed scenarios with simultaneous damage and sensor failure were set, as listed in Table 6. The sensor fault was introduced by artificially simulating the two common types of faults at different sensors simultaneously, as described in Section 2.1. The specific parameters of the sensor faults is listed in Table 7. Two Structural damage pattern plus the intact pattern are considered, also as listed in Table 6 and Fig. 18. For damage pattern 2, we fully loosened 6 bolts at mid-span joints of one longitudinal beam and tightened all the other bolts. For damage pattern 3, in order to simulate section loss, a 10 mm × 10 mm notch was made in the upper and lower flanges at the mid-span position of the specified UB beam, as shown in Fig. 18. Fig. 19 depicts some of the acceleration response time curves measured by sensor 1# under damage patterns 2 and 3.

Figure 20 demonstrates that the submodels of the SD-CNN group and the DI-CNN group are 100% and 82.71% accurate on average respectively. Furthermore, the individual submodels may achieve a structural damage identification performance of 99.12% or as low as 59.17% primarily because either the quality of the actual sensor data collected or the location of the deployment

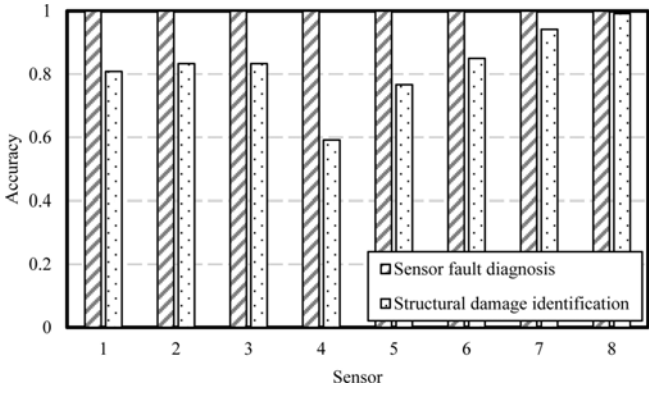

Fig. 20. The Diagnosis and Recognition Accuracy of Each Submodel

points affects the submodels of the DI-CNN group, and the obtained models offer different recognition performances at each measurement point. In addition, one-dimensional CNN submodels are influenced by the actual environment and may result in a certain degree of performance loss, possibly leading to false positives if relying on a single sensor to identify structural damage.

According to Table 6, three types of mixed scenarios were designed to validate the efficiency of the developed algorithm under the crossover conditions of sensor fault and structural damage. Fig. 21 presents the identification results. In mixed scenario-1 and mixed scenario-2, if the data obtained from the sensor network are directly fed into the DI-CNN group, the

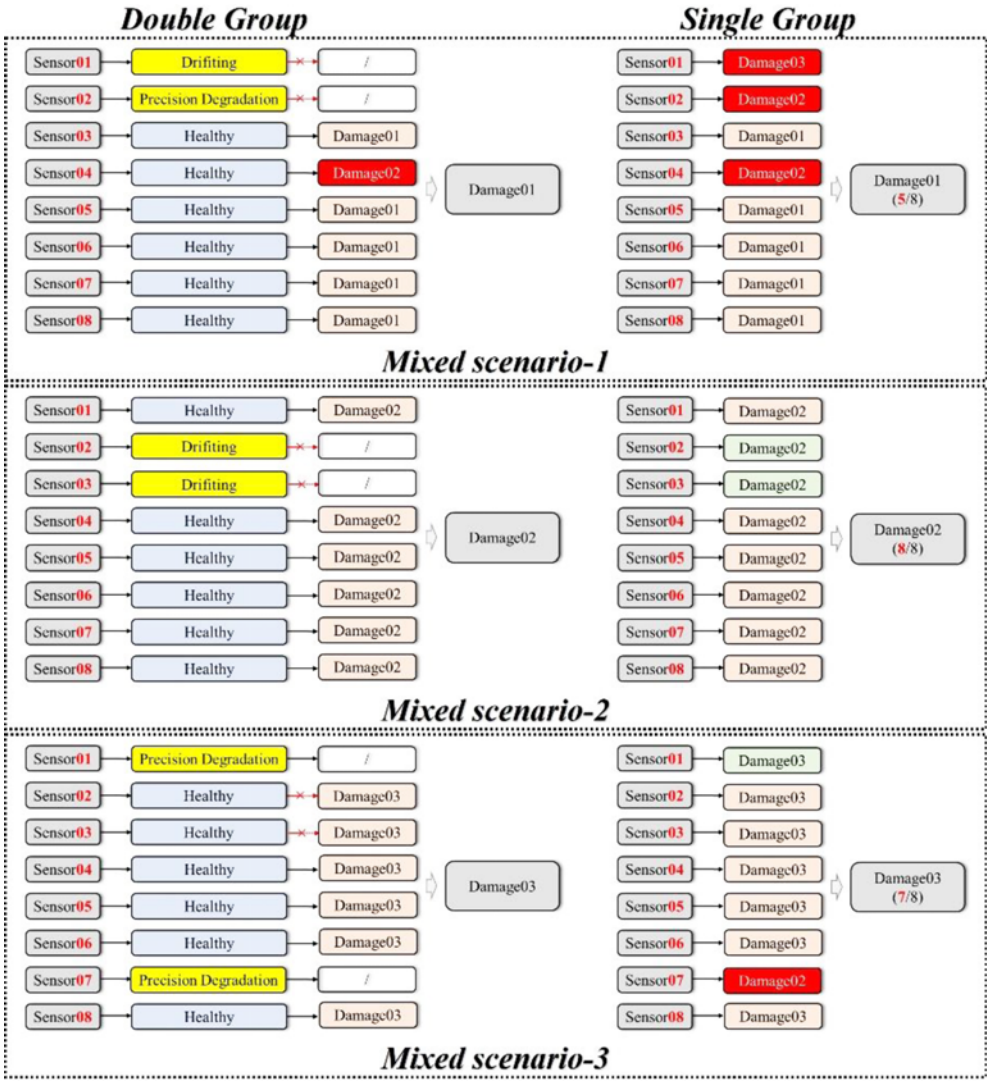

Fig. 21. The Results of the Identification of the Mixed Scenarios

discrimination results of sensors 1#, 2#, and 7# of the submodels may be misjudged due to the negative impact of the sensor fault models. However, the anomalous sensors are effectively identified and fed back when the SD-CNN group is added. Additionally, the results of the DI-CNN group are tallied by integrated voting, and the plural is assigned as the final result to avoid the variability of the performance of the submodels corresponding to sensor 4# and to further improve the reliability of the results of the structural damage identification. The computation time of the developed algorithm for the testing data set is 22.93 s. The computation times of the SD-CNN group and the DI-CNN group are also 11.41 and 11.52 s respectively, with average computation times of 94 and 105 ms for the two types of submodels, confirming that they have a high feedback rate.

5. Conclusions

This paper proposed a new method for structural damage identification based on a one-dimensional convolutional neural network group considering the sensor fault to reduce the misjudgment of the damage caused by the sensor fault. SHM benchmark data and laboratory experiments verified the validity of the proposed method. The main conclusions that follow from the findings of the current work are as follows:

1. The proposed algorithm has high computational efficiency and can satisfy the requirements of online damage identification for structural health monitoring. For SHM benchmark and Laboratory experiment cases, the identification time of all samples in the test set is 53.09 s and 22.93 s, respectively. For a single test sample, the average judgment time of each submodel in the SD-CNN group was 278 and 94 ms, and that of each submodel in the DI-CNN group was 294 and 105 ms, respectively.
2. By comparing the identification results of the two-layer groups, the developed SD-CNN group can diagnose the status of the sensor performance and truncate the faulty

signals participating in the damage identification by the DI-CNN group, which can enhance the efficiency of damage identification. In addition, the decision module is employed to analyze the identification results of the submodels of the DI-CNN group, which can reduce the influence of the misjudgment of the submodels on structural damage identification, thereby improving the accuracy of structural damage recognition.

Acknowledgments

The authors acknowledge the financial support from the National Natural Science Foundation of China (Grant No. 51808122): Natural Science Foundation of Fujian Province (Grant No. 2020J01580): and Key Laboratory for Structural Engineering and Disaster Prevention of Fujian Province (Huaqiao University) (Grant No. SEDPFJ-2018-01).

ORCID

Not Applicable

References

Altunışık AC, Okur FY, Karaca S, Kahya V (2019) Vibration-based damage detection in beam structures with multiple cracks: Modal curvature vs. modal flexibility methods. *Nondestructive Testing and Evaluation* 34(1):33-53, DOI: 10.1080/10589759.2018.1518445

Ananthi G, Msd B, Roy K, Lim J (2021) Influence of intermediate stiffeners on the axial capacity of cold-formed steel back-to-back built-up unequal angle sections – sciencedirect. *Structures* 32:827-848, DOI: 10.1016/j.istruc.2021.03.059

Ananthi G, Roy K, Lim J (2022) Behaviour and strength of back-to-back built-up cold-formed steel unequal angle sections with intermediate stiffeners under axial compression. *Steel & Composite Structures: An International Journal* 42(1):1-22, DOI: 10.12989/scs.2022.42.1.001

Azimi M, Eslamlou AD, Pekcan G (2020) Data-driven structural health monitoring and damage detection through deep learning: State-of-the-art review. *Sensors* 20(10):2778, DOI: 10.3390/s20102778

Boudiaf M, Rony J, Ziko M, Granger Eric, Pedersoli M, Piantanida P, Ayed BI (2020) A unifying mutual information view of metric learning: Cross-entropy vs. pairwise losses, *Computer Vision-ECCV*, 2020(12351):548-564, DOI: 10.1007/978-3-030-58539-6_33

Chi Y, Roy K, Chen B, Fang Z, Lim J (2021) Effect of web hole spacing on axial capacity of back-to-back cold-formed steel channels with edge-stiffened holes. *Steel & Composite Structures* 40(2):287-305, DOI: 10.12989/scs.2021.40.2.287

Ding YL, Ren P, Zhao HW, Miao CQ (2018) Structural health monitoring of a high-speed railway bridge: Five years review and lessons learned. *Smart Structures and Systems* 21(5):695-703, DOI: 10.12989/sss.2018.21.5.695

Flouri K, Saukh O, Sauter R, Jalsan KE, Bischoff R, Meyer J, Feltrin G (2012) A versatile software architecture for civil structure monitoring with wireless sensor networks. *Smart Structures and Systems* 10(3):209-228, DOI: 10.12989/sss.2012.10.3.209

Frank PM (1996) Analytical and qualitative model-based fault diagnosis–a survey and some new results. *European Journal of Control* 2(1):6-28, DOI: 10.1016/S0947-3580(96)70024-9

Fu Y, Peng C, Gomez F, Narazaki Y, Spencer BF (2019) Sensor fault management techniques for wireless smart sensor networks in structural health monitoring. *Structural Control and Health Monitoring* 26(7):e2362, DOI: 10.1002/stc.2362

Hüsem M, Nasery MM, Okur FY, Altunışık AC (2018) Experimental evaluation of damage effect on dynamic characteristics of concrete encased composite column-beam connections. *Engineering Failure Analysis* 91:129-150, DOI: 10.1016/j.engfailanal.2018.04.030

Jana D, Patil J, Herkal S, Nagarajaiah S (2022) CNN and convolutional autoencoder (CAE) based real-time sensor fault detection, localization, and correction. *Mechanical Systenms and Signal Processing* 2022(169):108723, DOI: 10.1016/j.ymssp.2021.108723

Johnson EA, Lam HF, Katafygiotis LS, Beck JL (2004) Phase I IASC-ASCE structural health monitoring benchmark problem using simulated data. *Journal of Engineering Mechanics* 130(1):3-15, DOI: 10.1061/(ASCE)0733-9399(2004)130:1(3)

Kahya V, Okur FY, Karaca S, Altunışık AC, Aslan M (2021) Multiple damage detection in laminated composite beams using automated model update. *Structure* 34:1665-1683, DOI: 10.1016/j.istruc.2021.08.117

Kingma D, Ba J (2015) ADAM: A method for stochastic optimization. *The 3rd International Conference for Learning Representations (ICLR)*, San Diego, May 7-9, USA: IEEE, 1-15, DOI: 10.48550/arXiv.1412.6980

Krizhevsky A, Sutskever I, Hinton GE (2012) Imagenet classification with deep convolutional neural networks. *Advances in Neural Information Processing Systems* 25:1097-1105, DOI: 10.1145/3065386

Kullaa J (2010) Sensor validation using minimum mean square error estimation. *Mechanical Systems and Signal Processing* 24(5):1444-1457, DOI: 10.1016/j.ymssp.2009.12.001

Kullaa J (2011) Distinguishing between sensor fault, structural damage, and environmental or operational effects in structural health monitoring. *Mechanical Systems and Signal Processing* 25(8):2976-2989, DOI: 10.1016/j.ymssp.2011.05.017

Kullaa J (2013) Detection, identification, and quantification of sensor fault in a sensor network. *Mechanical Systems and Signal Processing* 40(1):208-221, DOI: 10.1016/j.ymssp.2013.05.007

Li HN, Gao DW, Yi TH (2008) Advances in structural health monitoring systems in civil engineering. *Advances in Mechanics* 38(2):151-166, DOI: 10.1038/cgt.2008.5

Li LL, Liu G, Zhang LL, Li Q (2019) Sensor fault detection with generalized likelihood ratio and correlation coefficient for bridge SHM. *Journal of Sound and Vibration* 442:445-458, DOI: 10.1016/j.jsv.2018.10.062

Li LL, Liu G, Zhang LL, Li Q (2020) FS-LSTM-Based sensor fault and structural damage isolation in SHM. *IEEE Sensors Journal* 21(3):3250-3259, DOI: 10.1109/JSEN.2020.3022099

Li DL, Wang Y, Wang JX, Wang C, Duan YQ (2020) Recent advances in sensor fault diagnosis: A review. *Sensors and Actuators A: Physical* 309:111990, DOI: 10.1016/j.sna.2020.111990

Lin YZ, Nie ZH, Ma HW (2017) Structural damage detection with automatic feature-extraction through deep learning. *Computer-Aided Civil and Infrastructure Engineering* 32(12):1025-1046, DOI: 10.1111/mice.12313

Liu G, Li LL, Zhang LL, Li Q, Law SS (2020) Sensor faults classification for SHM systems using deep learning-based method with Tsfresh features. *Smart Materials and Structures* 29(7), DOI: 10.1088/1361-665X/ab85a6

Long J, Shelhamer E, Darrell T (2015) Fully convolutional networks for semantic segmentation. *Proceedings of the IEEE conference on computer vision and pattern recognition*, June 7-9, Boston, MA, USA, DOI: 10.1109/CVPR.2015.7298965

Mohamed L, Ibrahim AS (2002) Model-based fault diagnosis via parameter estimation using knowledge base and fuzzy logic approach. *11th IEEE Mediterranean Electrotechnical Conference*, May 7-9, Cairo, Egypt

Srivastava N, Hinton G, Krizhevsky A, Sutskever I, Salakhutdinov R (2014) Dropout: A simple way to prevent neural networks from overfitting. *The Journal of Machine Learning Research* 15(1):1929-1958, DOI: 10.5555/2627435.2670313

Zhan YL, Lu SJ, Xiang TY, Wei T (2021) Application of convolutional neural network in random structural damage identification. *Structures* 29:570-576, DOI: 10.1016/j.istruc.2020.11.056

Zhang T, Biswal S, Wang Y (2020) SHMnet: Condition assessment of bolted connection with beyond human-level performance. *Structural Health Monitoring* 19(4):1188-1201, DOI: 10.1177/1475921719881237

Zhao R, Yan R, Chen Z, Mao K, Wang P, Gao RX (2019) Deep learning and its applications to machine health monitoring, *Mechanical Systenms and Signal Processing* 115:213-237, DOI: 10.1109/MELECON.2002.1014644

Zhu HP, Yu J, Zhang JB (2011) A summary review and advantages of vibration-based damage identification methods in structural health monitoring. *Engineering Mechanics* 28(2):1-17, DOI: 10.6052/j.issn.1000-4750.2010.06.ST03